Video Article

Synthesis and Performance Characterizations of Transition Metal Single Atom Catalyst for Electrochemical CO_2 Reduction

Kun Jiang[1], Guangxu Chen[2], Haotian Wang[1]

[1]Rowland Institute, Harvard University

[2]Materials Science and Engineering, Stanford University

Correspondence to: Haotian Wang at hwang@rowland.harvard.edu

URL: https://www.jove.com/video/57380
DOI: doi:10.3791/57380

Keywords: Chemistry, Issue 134, Single atom catalyst, transition metal, electrospinning, graphene, carbon dioxide reduction, Faradaic efficiency

Date Published: 4/10/2018

Citation: Jiang, K., Chen, G., Wang, H. Synthesis and Performance Characterizations of Transition Metal Single Atom Catalyst for Electrochemical CO_2 Reduction. *J. Vis. Exp.* (134), e57380, doi:10.3791/57380 (2018).

Abstract

This protocol presents both the synthesis method of the Ni single atom catalyst, and the electrochemical testing of its catalytic activity and selectivity in aqueous CO_2 reduction. Different from traditional metal nanocrystals, the synthesis of metal single atoms involves a matrix material that can confine those single atoms and prevent them from aggregation. We report an electrospinning and thermal annealing method to prepare Ni single atoms dispersed and coordinated in a graphene shell, as active centers for CO_2 reduction to CO. During the synthesis, N dopants play a critical role in generating graphene vacancies to trap Ni atoms. Aberration-corrected scanning transmission electron microscopy and three-dimensional atom probe tomography were employed to identify the single Ni atomic sites in graphene vacancies. Detailed setup of electrochemical CO_2 reduction apparatus coupled with an on-line gas chromatography is also demonstrated. Compared to metallic Ni, Ni single atom catalyst exhibit dramatically improved CO_2 reduction and suppressed H_2 evolution side reaction.

Video Link

The video component of this article can be found at https://www.jove.com/video/57380/

Introduction

Converting CO_2 into chemicals or fuels using clean electricity is becoming increasingly important as a potential route to prevent further CO_2 emissions[1,2,3,4,5,6]. However, this practical application is currently challenged by the low activity and selectivity of CO_2 reduction reaction (CO_2RR) due to the high kinetic barriers and the competition with hydrogen evolution reaction (HER) in aqueous media. Most of the traditional transition metal catalyst, such as Fe, Co, and Ni, exhibit low CO_2RR selectivity due to their superb HER activities[7,8]. Effectively tuning their material properties to change the reaction pathways on these transition metal catalysts becomes critical to improve their CO_2RR selectivity. Among different methods to modify the electronic properties of catalysts, dispersing metal atoms into a single-atom morphology attracts intensive attentions recently due to their dramatically changed catalytic behaviors compared to their bulk counterpart[9,10,11]. However, due to the high mobility of unbounded atoms, it is quite challenging to obtain single metal atoms without the presence of supportive materials. Therefore, a host matrix material with defects created to confine and coordinate with transition metal atoms is necessary. This could open up new opportunities to: 1) tune the electronic properties of transition metals as CO_2RR active sites, and 2) at the same time maintain relatively simple atomic coordination for fundamental mechanism studies. In addition, those transition metal atoms trapped in a confined environment cannot be easily moved around during catalysis, which prevents the nucleation or reconstructions of surface atoms observed in many cases[12,13,14].

Two-dimensional layered graphene is of particular interest as host for metal single atoms due to their high electron conductivity, chemical stability, and inertness to both CO_2 reduction and HER catalytic reactions. More importantly, Fe, Co, and Ni metals were known to be able to catalyze the carbon graphitization process on their surface[15]. In short, those transition metals would alloy with carbon during the high temperature thermal annealing process. When the temperature drops, carbon starts to precipitate out of the alloying phase and is catalyzed to form graphene layers on the surface of transition metal. During this process, with graphene defects generated, metal single atoms would be trapped in those graphene defects as the active sites for CO_2RR[16,17,18,19]. Here, we report this detailed protocol intending to help new practitioners in the field of single atom catalysis, as well as to provide an explicit demonstration of on-line CO_2 reduction product analysis. More information can be found in our recently published article[19] and a series of related works[20,21,22,23].

Protocol

1. Preparation of Ni Single Atom Catalyst (NiN-GS)

1. Preparation of electrospinning precursor solution

1. Take a 20 mL scintillation vial, dissolve 0.5 g of polyacrylonitrile (M_w=150,000), 0.5 g of polypyrrolidone (M_w=1,300,000), 0.5 g of $Ni(NO_3)_2{\cdot}6H_2O$, and 0.1 g of dicyandiamide (DCDA) in 10 mL of dimethylformamide (DMF).
2. Heat the DMF mixture to 80 °C and keep the mixture at 80 °C with constant stirring until all polymers and salt are dissolved and a clear solution is observed.

2. Electrospinning to produce polymer fibers
   1. Set conventional electrospinning parameters as: 15 kV of static electric voltage, 15 cm of air gap distance, a collection substrate of 8 × 8 cm carbon fiber paper (CFP) with - 4 kV electric voltage.
   2. Extract 5 mL of precursor solution into a 5 mL syringe, start syringe pump at a flow rate of 1.2 mL h^{-1}, then start the electrospinning.
      NOTE: A high voltage is used for electrospinning. Even though very low current goes through the system during spinning process, an insulated wood cabinet is suggested.
   3. Take out the CFP substrate once the electrospinning process is finished. A polymer fiber film covers the CFP surface.

3. Annealing polymer fibers into carbon nanotubes
   1. Heat the as-prepared polymer fiber film/CFP to 300 °C in 1.5 h in a box furnace, and keep the temperature for 0.5 h to oxidize the polymers.
      NOTE: After the oxidization process, the nanofibers (NFs) are self-detached from the carbon paper resulting in the freestanding film.
   2. Use a pair of scissors to cut those nanofibers into smaller pieces (~ 0.5 cm × 2cm) and place them into a quartz boat.
   3. Place the quartz boat into a tube furnace, and deaerate it within forming gas (5% H_2 in Ar) atmosphere. Keep the gas flow rate as 100 sccm and the pressure as 1 Tor.
   4. Heat up within 10 min ramping to 300 °C, and 2 h ramping to 750 °C, where it is maintained for another 1 h and followed by the natural cooling down.

4. Ball mill as-synthesized NiN-GS catalyst for 5 min to nanopowders for catalysis and characterizations.

2. Electrochemical CO_2 Reduction Measurements

1. Cell and Electrodes
   1. To prepare 0.1 M $KHCO_3$ electrolyte for the following measurements, first dissolve 2.5 g of $KHCO_3$ in 250 mL of ultrapure water, then purify the electrolyte by electrolysis between two graphite rods at 0.1 mA for 24 h to remove any trace amount of metal ions.
   2. Take a fresh (electrochemically) polished glassy carbon (1 cm × 2 cm), and cover its backside with an electrochemically inert, hydrophobic wax, as the working electrode substrate.
   3. Take a 4 mL scintillation vial, mix 5 mg of as-prepared NiN-GS catalyst with 1 mL of ethanol and 100 µL of ionomer solution (5% in 2-proponal) within the vial, and sonicate for 20 min to get a homogeneous catalyst ink suspension.
   4. Pipet 80 µL of the catalyst ink onto 2 cm^2 glassy carbon surface (0.2 mg cm^{-2} mass loading), and vacuum dry the catalyst covered electrode in a desiccator prior to usage.
   5. Use a platinum foil and a saturated calomel electrode (SCE) as the counter and reference electrode, respectively.
   6. Use a customized gastight H-type glass cell, separated by proton exchange membrane, for the above 3 electrodes assembling as well as the electrochemical tests running.
   7. Place the working electrode and SCE reference electrode in one compartment of H-cell, and Pt foil electrode in the other chamber. Inject ~ 25 mL of electrolyte in each compartment of H-cell.
   8. Connect the 3 electrodes in H-cell to the electrochemical work station for potential control.
   9. Bubble the electrolyte with N_2 at 50.0 sccm (monitored by mass flow controller) for 30 min toward N_2-saturated 0.1 M $KHCO_3$.
   10. Select Cyclic Voltammetry (CV) technique in EC-Lab software, set "E Range (potential)" as "-10 V to 10 V", "I Range (current)" as "Auto", perform 5 continuous CV scans from -0.5 V to -1.8 V (vs. SCE) at a scan rate of 50 mV/s in N_2-saturated 0.1 M $KHCO_3$.
   11. Change to 50 sccm CO_2 gas flow, wait for 30 min toward CO_2-saturated 0.1 M $KHCO_3$ electrolyte and maintain the same CO_2 flow throughout the following electrolysis.
   12. Select CV technique in EC-Lab software, set "E Range (potential)" as "-10 V to 10 V", "I Range (current)" as "Auto", perform 5 continuous CV scans from -0.5 V to -1.8 V (vs. SCE) at a scan rate of 50 mV/s in CO_2-saturated 0.1 M $KHCO_3$.
   13. Use a pH Meter to determine the pH values of electrolytes, *i.e.*, 0.1 M $KHCO_3$ saturated with either N_2 or CO_2.
   14. Convert all potentials measured against SCE to the reversible hydrogen electrode (RHE) scale in this work using E (vs RHE) = E (vs SCE) + 0.244 V + 0.0591 × pH.
   15. Determine solution resistance (R_u) in EC-Lab software by selecting Potentiostatic Electrochemical Impedance Spectroscopy (PEIS) technique, then set frequency range from 0.1 Hz to 200 kHz, record the resistance value.
   16. Manually compensate *iR*-drop as E (iR corrected vs RHE) = E (vs RHE) - R_u × I (amps of average current).

2. CO_2 reduction products analysis by on-line gas chromatograph (GC)
   1. Employ a GC, equipped with a combination of molecular sieve 5A and micropacked columns, for gas products analysis during CO_2RR.
      NOTE: The detailed GC column types can be found in attached **Table of Materials**.
   2. Use a thermal conductivity detector (TCD) to quantify H_2 concentration, and a flame ionization detector (FID) with a methanizer to quantitative analysis CO content and/or any other alkane species.
   3. Use two different standard gases for the calibration curves of H_2 and CO concentration (H_2: 100 and 1042 ppm; CO: 100 and 496.7 ppm; balanced with Argon).
   4. During electrolysis, maintain CO_2 gas flow rate at 50.0 sccm, deliver CO_2 into the cathodic compartment containing CO_2-saturated 0.1 M $KHCO_3$ electrolyte, and vent the exhaust into GC.
   5. Stepwise tune the voltage on working electrode, ranging from -0.3 to -1.0 V vs. RHE, keep ~ 15 min for each potential and record the corresponding chronoamperimetric curve.
   6. Determine the H_2 and CO contents in the exhaust from TCD and FID signals, respectively.
      NOTE: The gas products are sampled after a continuous electrolysis of ~ 10 min under each potential. The 50 sccm CO_2 gas, mixed with continuously produced H_2 and CO, flowed through the sampling loop (1 mL) of GC during the electrolysis.

7. Calculate the partial current density for a given gas product as below:

$$j_i = x_i \times v \times \frac{n_i F p_0}{RT} \times (electrode\ area)^{-1}$$

where x_i is the volume fraction of certain product determined by online GC referenced to calibration curves from two standard gas samples (Scott and Airgas), v is the flow rate of 50 sccm, n_i is the number of electrons involved, p_0 = 101.3 kPa, and F is the Faradaic constant and R is the gas constant.

8. Calculate the corresponding Faradaic efficiency (FE) at each potential as $FE = j_i / i_{total} \times 100\ \%$.

NOTE: The overall Faradaic efficiency could be within a range of 90 to 110% due to the errors from gas flow rate, current density, and gas concentration analysis on GC.

Representative Results

Scanning electron microscopy (SEM), scanning transmission electron microscopy (STEM) and energy-dispersive X-ray spectroscopy (EDX) mapping images are shown in **Figure 1** for the morphology characterization of NiN-GS. Three-dimensional atom probe tomography (3D-APT) results are shown in **Figure 2** for the direct identification of single Ni sites distribution as well as their neighboring chemical environment. On-line electrochemical GC measurements setup and result are shown in **Figure 3** for the quantification of CO_2RR gas products.

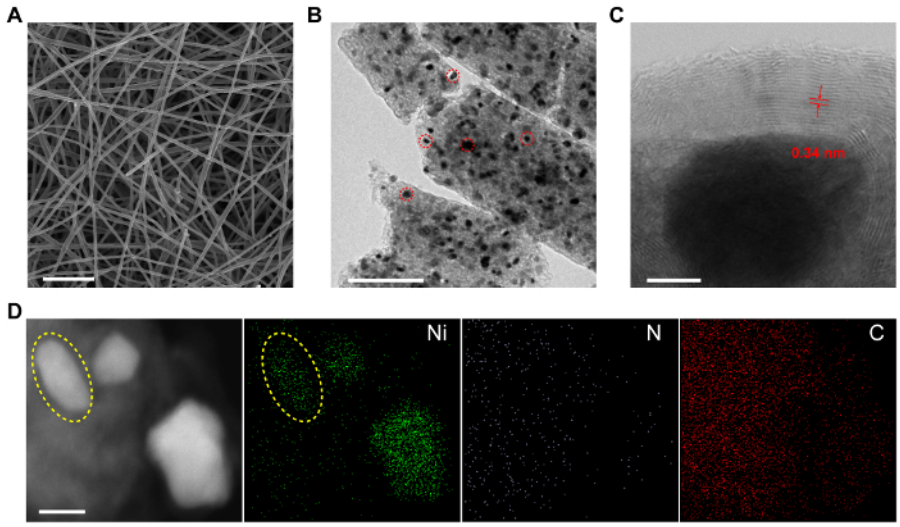

Figure 1: Characterizations of NiN-GS catalysts. (A) SEM image of carbonized electrospin polymer NFs. Scale bar: 5 μm. (B) TEM image of ball-milled NiN-GS catalyst. The dark dots (pointed out by red circles as examples) uniformly distributed in the CNF are Ni nanoparticles (NPs). Scale bar: 200 nm. (C) Aberration-corrected STEM image of a Ni NP tightly wrapped by a few graphene layers. The Ni NP is ~ 20 nm in diameter. The GS is ~ 10 nm thick. The layer spacing is measured to be 0.34 nm. Scale bar: 5 nm. (D) EDS mapping of NiN-GS catalyst. Three Ni NPs were observed in the STEM image on the left panel, which is consistent with the Ni mapping image with one of the NPs indicated by the yellow circle. Ni signals were detected in areas away from the NPs, demonstrating the successful incorporation of Ni atoms in graphene layers. Scale bar: 20 nm. This figure has been modified from Reference 19 with copyright permission from Elsevier 2017. Please click here to view a larger version of this figure.

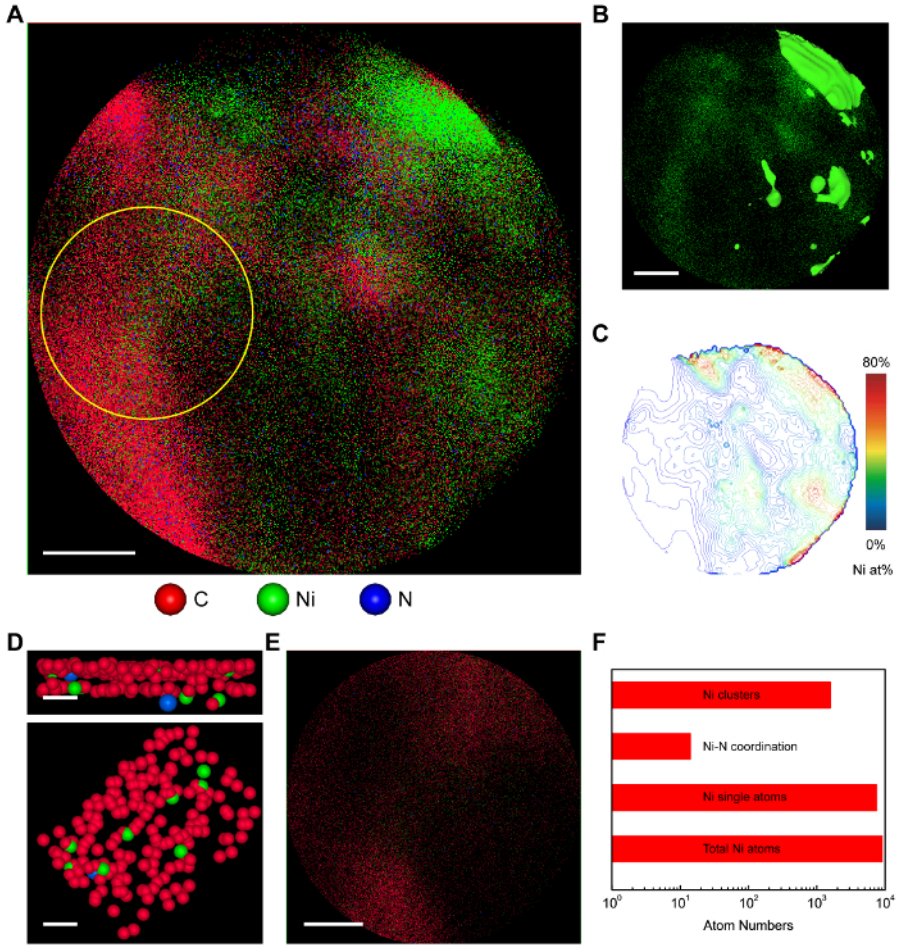

Figure 2: Atom probe tomography of NiN-GS catalyst. (A) The 2D atom map of NiN-GS. Scale bar: 10 nm. (B) The 2D projected view of Ni atoms. The green areas represent Ni rich areas (> 50 at%). Away from the Ni sources, there are still a significant number of Ni atoms dispersed in the carbon area. Scale bar: 10 nm. (C) The contour map of Ni concentration with an interval of 2 at%. (D) Zoomed in side-view (upper) and top-view (lower) graphene layers with Ni single atoms coordinated in vacancies. Only one Ni atom is directly coordinated with one N atom. Scale bars: 1 nm. (E) Atom map of the selected area in **Figure 2A** as pointed out by the yellow circle. Scale bar: 5 nm. (F) The statistic of the selected area in **Figure 2E**. Most of the Ni atoms are in single-atom morphology, and 0.2% of them are coordinated with N atoms. This figure has been modified from Reference 19 with copyright permission from Elsevier 2017. Please click here to view a larger version of this figure.

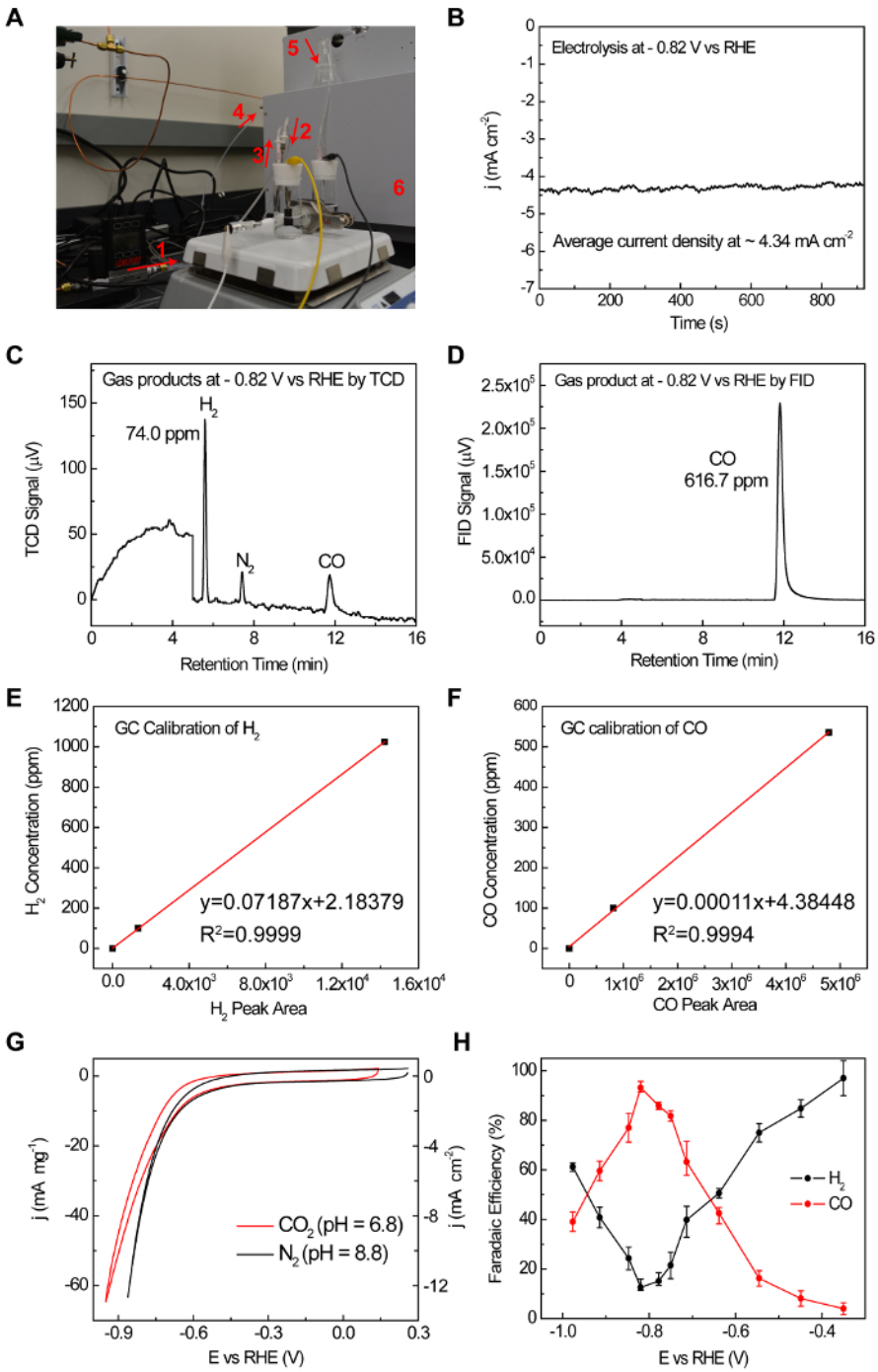

Figure 3: The GC measurement set up and a representing example to demonstrate the whole process of FE measurement. (A) 1. Mass flow control (MFC) for an accurate 50 sccm CO_2 flow rate. 2. CO_2 gas flows into the cell. 3. CO_2 gas flows out of the reactor bringing gas products together. 4. The gas mixture fills the sampling loop of GC continuously. 5. The continuous gas flow is monitored by the bubbles generated in the glass. (B) Chronoamperometry of CO_2 reduction under -0.82 V vs RHE. (C, D) TCD and FID responses to the gas products. (E, F) TCD and FID standard gas calibration. (G) CVs of NiN-GS in CO_2 and N_2 saturated electrolyte, suggesting a different reaction pathway when CO_2 is present. (H) FEs of H_2 and CO under different applied potentials for NiN-GS. This figure has been modified from Reference 19 with copyright permission from Elsevier 2017. Please click here to view a larger version of this figure.

Discussion

In the above electrospinning process, two important steps should be noted in material synthesis procedures: 1) heating the DMF mixture (step 1.1.2), and 2) the pump rate adjusting (step 1.2.2) to match the spinning rate. The SEM image in **Figure 1A** shows the obtained carbon nanofibers interconnected with each other (~200 nm in diameter). They were broken into small pieces by ball milling for characterizations as shown in **Figure 1B**. Ni nanoparticles were uniformly distributed in the carbon nanofibers. Carbon atoms alloyed with Ni under high temperature

would precipitate out and were catalyzed to form graphene layers on the Ni metal surface during the cooling down process. A closer observation of the Ni NPs by aberration-corrected STEM in **Figure 1C** reveals that, the NP is tightly encapsulated by a few layers (~ 10 nm) of graphene as confirmed by the averaged layer spacing of ~ 0.34 nm. No Ni clusters were observed within the GS. This shell prevents the Ni NP from a direct contact with the aqueous electrolyte and can thus dramatically suppress HER. The existence of Ni atoms in the surface shell was confirmed by energy-dispersive X-ray spectroscopy (EDS) mapping in **Figure 1D**. The Z-contrast STEM image on the left panel shows three bright areas representing three Ni NPs, with one of them pointed out by the yellow circle. In the Ni mapping image (marked by green dots), in addition to the NP regions with concentrated signals, Ni peaks was also detected in the neighboring carbon areas, demonstrating the successful incorporation of Ni atoms in the GS. N doping here plays a critical role in creating defects in the graphene layers, which helps to trap and bond a significant number of Ni atoms in the GS. Those coordinated Ni atoms within the graphene layers in NiN-GS showed distinctively different oxidation states from Ni NPs covered below by X-ray photoelectron spectroscopy, suggesting the successful tuning of Ni electronic structures and thus the possible tuning of its catalytic activities. Besides, those Ni single atoms trapped in confined graphene matrix cannot be easily moved around during practical applications, which circumvents the catalyst structural reconstructions in harsh reaction conditions.

Although some previous studies suggested CO_2-to-CO catalysis on metal-nitrogen-carbon sites, few evidence to date was reported to demonstrate the single-atom morphology or the coordination environment of the active sites. Herein, a direct evidence of the Ni single atoms coordinated in graphene vacancies is obtained by the three-dimensional (3D) atomic-resolution atom probe tomography (APT) characterization, which is able to reveal whether those Ni atoms are isolated single-atoms or small clusters, and whether those Ni atomic sites are coordinated with N or not. The projected 2D image of the 3D tomography of NiN-GS catalyst was shown in **Figure 2A**. Each pixel represents one single atom. As shown in **Figure 2B**, away from the areas with concentrated Ni NPs, there are also a significant number of Ni atoms dispersed in carbon, consistent with our EDX mapping in **Figure 1D**. The contour map with an interval of 2 at% in **Figure 2C** provides detailed distribution information of Ni atoms in the catalyst, with decreased Ni atom concentrations away from the Ni sources. Local coordination environment of Ni atoms was shown by taking a closer look at graphene layers in **Figure 2D**. There are a few Ni single atoms coordinated in graphene vacancies, providing a direct evidence of the single Ni atomic site. No Ni clusters were observed. In addition, we also noticed that there is one Ni atom coordinated with one N atom in graphene vacancy, suggesting a small ratio of Ni atomic sites coordinated with N atoms. More detailed information about the surrounding coordination of Ni atomic sites can be extracted from statistics and quantitative analysis (**Figure 2F**). The selected area with dispersed Ni atoms is indicated by the yellow circle in **Figure 2A** and enlarged in **Figure 2E**. Among all of the Ni atoms in this area, 83% of them are in single atoms, without neighboring Ni atoms closer than 2.2 Å. In addition, in those Ni single atoms, only 0.2% of them are directly coordinated with one neighboring N (less than 2 Å), suggesting that most of the Ni atomic sites are coordinated with C atoms. More detailed experimental approach including synchrotron-based X-ray absorption spectroscopy characterization, *in situ* electrochemical attenuated total reflectance infrared spectra (ATR-IR) with CO as surface probe, together with other control experiments design and density functional theory (DFT) simulations of CO_2-to-CO reduction over different coordination moieties, are carried out to comprehensively probe the active center of Ni single atom sites and these results can be found in Jiang, K. *et al.*[19].

The electrocatalytic CO_2RR performance of NiN-GS catalyst, drop casted on glassy carbon current collector, is performed in 0.1 M $KHCO_3$ electrolyte in a customized H-cell. Gas products are analyzed by GC at potential steps of 100 mV and further zoomed into 50 mV around the FE peak. Note that the concentration of gas products can be tuned by changing the CO_2 gas flow rate (step 2.2.4) and therefore the FE measurements can be accurate even for small currents. Taking the chronoamperometric test of CO_2 reduction under -0.82 V vs RHE for example (**Figure 3B**), after the gas flow goes into sampling loop, H_2 is detected at ~5.5 min by TCD, and CO is detected at ~12 min by FID, corresponding to a CO FE of ~93% and H_2 FE of ~12%. Given the diverse CO_2RR products distribution, the present online GC setup thus provides valuable information on the real-time tracking exhaust content during electrolysis.

In summary, we've demonstrated a method for incorporating transition metal atoms into a well-defined two-dimensional matrix and effectively tuning their electronic structures and thus favoring the desired CO_2RR pathways. The protocol of CO_2RR gas product analysis provides a detailed and standard method to accurately measure the Faradaic efficiency of each product. Given the wide variety of single atom catalyst applications, the present protocol consisting facile catalyst preparation and online products analysis provides an important platform for designing various robust transition metal single atom catalysts to fulfill more efficient renewable energy conversion and chemical industrial demands.

Acknowledgements

This work was supported by the Rowland Fellows Program at the Rowland Institute of Harvard University. This work was performed in part at the Center for Nanoscale Systems (CNS), a member of the National Nanotechnology Infrastructure Network, which is supported by the National Science Foundation under award no. ECS-0335765. The CNS is part of Harvard University.

References

1. Lewis, N. S., & Nocera, D. G. Powering the planet: Chemical challenges in solar energy utilization. *P. Natl. Acad. Sci. USA.* **103**, 15729-15735 (2006).
2. Appel, A. M. *et al.* Frontiers, Opportunities, and Challenges in Biochemical and Chemical Catalysis of CO2 Fixation. *Chem. Rev.* **113**, 6621-6658 (2013).
3. Jhong, H. R., Ma, S. C., & Kenis, P. J. A. Electrochemical conversion of CO_2 to useful chemicals: current status, remaining challenges, and future opportunities. *Curr. Opin. Chem. Eng.* **2**, 191-199 (2013).
4. Ashford, D. L. *et al.* Molecular Chromophore-Catalyst Assemblies for Solar Fuel Applications. *Chem. Rev.* **115**, 13006-13049 (2015).
5. Nocera, D. G. Solar Fuels and Solar Chemicals Industry. *Accounts. Chem. Res.* **50**, 616-619 (2017).
6. Larrazabal, G. O., Martin, A. J., & Perez-Ramirez, J. Building Blocks for High Performance in Electrocatalytic CO_2 Reduction: Materials, Optimization Strategies, and Device Engineering. *J. Phys. Chem. Lett.* **8**, 3933-3944 (2017).
7. Hori, Y., Wakebe, H., Tsukamoto, T., & Koga, O. Electrocatalytic Process of Co Selectivity in Electrochemical Reduction of Co2 at Metal-Electrodes in Aqueous-Media. *Electrochim. Acta.* **39**, 1833-1839 (1994).
8. Hori, Y. in *Modern aspects of electrochemistry.* 89-189 Springer (2008).

9. Lin, S. *et al*. Covalent organic frameworks comprising cobalt porphyrins for catalytic CO2 reduction in water. *Science.* **349**, 1208-1213 (2015).
10. Zhang, X. *et al.* Highly selective and active CO2 reduction electrocatalysts based on cobalt phthalocyanine/carbon nanotube hybrid structures. *Nat. Commun.* **8**, 14675 (2017).
11. Zhao, C. M. *et al.* Ionic Exchange of Metal Organic Frameworks to Access Single Nickel Sites for Efficient Electroreduction of CO_2. *J. Am. Chem. Soc.* **139**, 8078-8081 (2017).
12. Manthiram, K., Beberwyck, B. J., & Aivisatos, A. P. Enhanced Electrochemical Methanation of Carbon Dioxide with a Dispersible Nanoscale Copper Catalyst. *J. Am. Chem. Soc.* **136**, 13319-13325 (2014).
13. Yang, M. *et al.* Catalytically active Au-O(OH)(x)-species stabilized by alkali ions on zeolites and mesoporous oxides. *Science.* **346**, 1498-1501 (2014).
14. Manthiram, K., Surendranath, Y., & Alivisatos, A. P. Dendritic Assembly of Gold Nanoparticles during Fuel-Forming Electrocatalysis. *J. Am. Chem. Soc.* **136**, 7237-7240 (2014).
15. Amini, S., Garay, J., Liu, G., Balandin, A. A., & Abbaschian, R. Growth of large-area graphene films from metal-carbon melts. *J. Appl. Phys.* **108**, 094321 (2010).
16. Krasheninnikov, A. V., Lehtinen, P. O., Foster, A. S., Pyykkö, P., & Nieminen, R. M. Embedding Transition-Metal Atoms in Graphene: Structure, Bonding, and Magnetism. *Phys. Rev. Lett.* **102**, 126807 (2009).
17. Jiang, K., Siahrostami, S., Zheng, T., Hu, Y., Hwang, S., Stavitski, E., Peng, Y., Dynes, J., Gangishetty, M., Su, D., Attenkofer, K., & Wang, H. Isolated Ni Single Atoms in Graphene Nanosheets for High-performance CO_2 Reduction. *Energy Environ. Sci.* Advance Article (2018).
18. Rodríguez-Manzo, J. A., Cretu, O., & Banhart, F. Trapping of Metal Atoms in Vacancies of Carbon Nanotubes and Graphene. *ACS Nano.* **4**, 3422-3428 (2010).
19. Jiang, K. *et al.* Transition metal atoms in a graphene shell as active centers for highly efficient artificial photosynthesis. *Chem.* **3**, 950-960 (2017).
20. Jiang, K., Wang, H., Cai, W. B., & Wang, H. T. Li Electrochemical Tuning of Metal Oxide for Highly Selective CO_2 Reduction. *ACS Nano.* **11**, 6451-6458 (2017).
21. Jiang, K. *et al.* Silver Nanoparticles with Surface-Bonded Oxygen for Highly Selective CO2 Reduction. *ACS Sustain Chem. Eng.* **5**, 8529-8534 (2017).
22. Siahrostami, S. *et al.* Theoretical Investigations into Defected Graphene for Electrochemical Reduction of CO_2. *ACS Sustain Chem. Eng.* **5**, 11080-11085 (2017).
23. Jiang, K. *et al.* Metal Ion Cycling of Cu Foil for Selective C-C Coupling in Electrochemical CO2 Reduction. *Nat. Catal.* (2017).

